SEISMIC RESERVOIR CHARACTERIZATION IN OFFSHORE NILE DELTA. PART II: PROBABILISTIC PETROPHYSICAL-SEISMIC INVERSION

M. Aleardi[1], F. Ciabarri[2], B. Garcea[2], A. Mazzotti[1]
[1] *Earth Sciences Department, University of Pisa, Italy*
[2] *EDISON, Milano, Italy*

Introduction. Reservoir characterization plays an essential role in integrated exploration and reservoir studies, as it provides an optimal understanding of the reservoir internal architecture and properties. In reservoir characterization studies seismic reflection data are often used to derive petrophysical rock properties (water saturation, porosity, shale content) from elastic parameters (seismic velocities, rock density or impedances). The rock-physics model is the link between elastic properties and such petrophysical parameters and it can be based on theoretical rock-physics equations or on empirical set of equations derived from available information (well-log or core data) and valid for the specific case of interest.

The inverse problem of estimating petrophysical properties from seismic reflection data is multidimensional, ill posed and strongly affected by noise and measurement errors. Therefore, the statistical approach to seismic reservoir characterization has become the most popular approach. It is able to take into account the uncertainties associated with the simplified rock-physics model, the error in the seismic data, and the natural variability of the petrophysical properties in the subsurface. The goal of this approach is to predict the probability of petrophysical variables when seismic velocities or impedances and density are assigned, and to capture the heterogeneity and complexity of the rocks and the uncertainty associated with the rock-physics model. For many examples of applications of this approach to reservoir characterization studies constrained by seismic and well-log data, see for example Avseth *et al*. (2005).

In this paper, we apply a two-step procedure to seismic reservoir characterization. The first step is a Bayesian linearized amplitude versus angle inversion (AVA) in which, on the line of Buland and Omre (2003) and Chiappa and Mazzotti (2009), we derive the elastic properties of the subsurface and their associated uncertainties assuming Gaussian-distributed errors and Gaussian-distributed elastic characteristics. The second step is a petrophysical inversion that uses the outcomes of AVA inversion, the previously defined rock-physics model, their associated uncertainties and the prior distribution of the petrophysical variables, to derive the probability distributions of the petrophysical properties in the target zone. The derivation and the calibration of different rock-physics models is the topic of the companion paper titled "*Seismic reservoir characterization in offshore Nile Delta. Part I: Comparing different methods to derive a reliable rock-physics model*". In that paper the empirical, linear, rock-physics model derived with a multilinear stepwise regression (named SR in the companion paper) and the theoretical rock-physics model (named TRPM in the companion paper) demonstrated to be the most reliable in predicting the elastic characteristics from the petrophysical properties. Then, the two rock-physics models are applied in the petrophysical inversion described here. In the context of petrophysical inversion, the main difference of applying a linear or a non-linear rock-physics model lies in the fact that the former allows the joint distribution of petrophysical and elastic properties to be analytically computed, while the latter requires a Monte Carlo simulation to derive such joint distribution.

We start with a brief theoretical description of the method and with a synthetic example based on actual well-log measurements. This test aims to demonstrate the applicability of the inversion method and to illustrate and compare the different results obtained by considering the empirical and the theoretical rock-physics models. Moreover, this synthetic test allows us to check the applicability and the reliability of the two rock-physics models in the specific case under examination. Then, a field case inversion is discussed. This inversion is performed for a single CMP location where well-control is available to validate the results.

The method. In the following discussion we will use *m* to indicate the elastic properties, typically P and S-impedance (*Ip* and *Is*, respectively) and density, *R* to indicate the petrophysical properties, such as water saturation (*Sw*), porosity (ϕ) and shaliness (*Sh*), whereas d_{obs} indicates the observed seismic data (typically the measured AVA responses). The method we use is a two-step procedure: a Bayesian linearized AVA inversion followed by a probabilistic petrophysical inversion. This petrophysical inversion makes use of the a-priori distribution of the petrophysical properties *p(R)* derived on the basis of well-log data, of the previously defined rock-physics model and of the results of AVA inversion to derive the probabilistic distribution of the petrophysical properties in the subsurface.

The first step of the petrophysical-seismic inversion is the Bayesian AVA inversion that jointly estimates the posterior distributions of the elastic properties in the subsurface by making use of a reformulation of the linear approximation of the Zoeppritz equation derived by Aki and Richards (1980). In particular, we parameterize the inversion in terms of P and S-impedance (*Ip* and *Is*, respectively) and density. In terms of impedances, the P-wave reflection coefficient *Rpp* as a function of the reflection angle (θ) can be written as follows:

$$Rpp(\theta) = \frac{1}{2\cos^2(\theta)}\frac{\Delta Ip}{\overline{Ip}} - 4\frac{\overline{Is}^2}{\overline{Ip}^2}\sin^2(\theta)\frac{\Delta Is}{\overline{Is}} + \left(\frac{1}{2} - \frac{1}{2\cos^2(\theta)} + 2\frac{\overline{Is}^2}{\overline{Ip}^2}\sin^2(\theta)\right)\frac{\Delta\rho}{\overline{\rho}} \qquad (1)$$

where $\overline{Ip}$, $\overline{Is}$ *and* $\overline{\varrho}$ are, respectively, the averages of impedances and density at the reflecting interface, whereas ΔIp, ΔIs and $\Delta\varrho$ are the corresponding contrasts. However, density estimates are not used in the petrophysical inversion since they are obviously correlated with the impedances ones and because the linear AVA inversion cannot retrieve reliable information about density with realistic noise levels (Buland and Omre, 2003). Following Stolt and Weglein (1985), the single-interface reflection coefficient in Eq. 1 can be easily extended to a time-continuous reflectivity function. The elastic properties estimated by Bayesian AVA inversion are delivered according to the following posterior probability distribution:

$$p(m \mid d_{obs}) = G(\mu_{m|dobs}, \Sigma_{m|dobs}) \qquad (2)$$

where: *G* indicates the Gaussian distribution where the posterior expectation and the covariance are equal to $\mu_{m|dobs}$ and $\Sigma_{m|dobs}$, respectively. The a-priori distributions and the vertical correlation of the elastic properties, needed to derive the posterior distribution in Eq. 2, can be determined from available well-log data. For full details about the Bayesian linearized AVA inversion see Buland and Omre (2003).

For what concerns the petrophysical inversion, we apply the method proposed by Grana and Della Rossa (2010) and briefly summarized in the following. Considering all variables as random vectors, we can write the rock-physics model (f_{RPM}) as:

$$m = f_{RPM}(R) + \varepsilon \qquad (3)$$

where: ε is the random error that describes the accuracy of the rock-physics model and can be determined by comparing the available well-log data with the predicted data. For the prior distribution of the petrophysical properties *p(R)* we assume a multivariate Gaussian mixture (GM) that is a linear combination of Gaussian distributions:

$$p(R) = \sum_{k=1}^{Nc} a_k G(\mu_R^k, \Sigma_R^k) \qquad (4)$$

where: *Nc* indicate the number of components of the mixture and a_k are the weights associated with each component (with $\sum_{k=1}^{Nc} a_k = 1$). Generally, each component is a specific litho-fluid class previously determined from available log data and from the geological knowledge of the investigated area. In this work, we consider three litho-fluid classes that are gas-sand, brine-sand and shale. The technique we adopt, to estimate the parameters of the Gaussian components

and the weights of the mixture, is the expectation maximization algorithm (Hastie *et al.*, 2005). This Gaussian mixture model allows us to describe the multimodality and the correlation that often characterize the distribution of the petrophysical properties in the subsurface.

If we assume that ε is Gaussian with zero mean and covariance $\Sigma\varepsilon$, the conditional probability $p(m|R)$ can be expressed as:

$$p(m \mid R) = G(f_{RPM}(R) + \varepsilon, \sum_{\varepsilon}) \tag{5}$$

where: $\Sigma\varepsilon$ can be estimated by comparing actual and predicted well-log data and is assumed independent from R and only related to ε. Note that this formulation allows us to account for uncertainties associated with the rock-physics model predictions that are expressed by ε and $\Sigma\varepsilon$.

The joint distribution of the elastic and the petrophysical properties is again a Gaussian mixture:

$$p(m, R) = \sum_{k=1}^{Nc} b_k G(\mu_{(m,R)}^k, \sum_{(m,R)}^k) \tag{6}$$

If the rock-physics model f_{RPM} is linear, this joint distribution can be derived analytically from the prior distribution $p(R)$. Conversely, if f_{RPM} is not linear the joint distribution $p(m,R)$ can be obtained from a semi-analytical approach that makes use of Monte Carlo samples. This last approach applies the expectation maximization algorithm to Monte Carlo samples to compute the characteristics of the joint distribution (see Grana and Della Rossa, 2010, for full details). Since the joint distribution is a Gaussian mixture, the conditional distribution $p(R|m)$ is again a Gaussian mixture and can be written as follows:

$$p(R \mid m) = \sum_{k=1}^{Nc} c_k G(\mu_{R|m}^k, \sum_{R|m}^k) \tag{7}$$

in which $\mu_{R|m}^k$ and $\sum_{R|m}^k$ are analytically computed from the joint distribution $p(m,R)$, from the prior model $p(R)$ and from the results (m) of Bayesian AVA inversion:

$$\mu_{R|m}^k = \mu_R^k + \sum_{R,m}^k (\sum_{m,m}^k)^{-1} (m - \mu_m^k) \tag{8}$$

and

$$\sum_{R|m}^k = \sum_{R,R}^k - \sum_{R,m}^k (\sum_{m,m}^k)^{-1} \sum_{m,R}^k \tag{9}$$

The weights c_k in the conditional GM distribution $p(R|m)$ can be computed as follows:

$$c_k(m) = \frac{b_k G(\mu_{R|m}^k, \sum_{R|m}^k)}{\sum_{l=1}^{Nc} b_l G(\mu_{R|m}^l, \sum_{R|m}^l)} \tag{10}$$

To compute the final conditional probability $p(R|d_{obs})$, which expresses the probability of petrophysical variables conditioned by seismic data, we need to propagate the uncertainties that characterize the results of the Bayesian AVA inversion into the conditional probability $p(R|m)$. To this end the Chapman-Kolmogorov equation can be used (Papoulis, 1984):

$$p(R \mid d_{obs}) = \int P(R \mid m) P(m \mid d_{obs})\, dm \tag{11}$$

This conditional probability is the final result of the petrophysical inversion conditioned by seismic data.

Results. To define the number of components of the a-priori Gaussian mixture distribution of the petrophysical properties ($p(R)$; Eq. 4) we consider three different litho-fluid facies that are shale, brine sand and gas sands. These facies are defined on the basis of available well-log data and geological knowledge of the investigated area. This trivariate Gaussian mixture allows us to account for correlations observed between petrophysical variables in each litho-fluid class. The parameters that define this GM distribution were obtained applying the

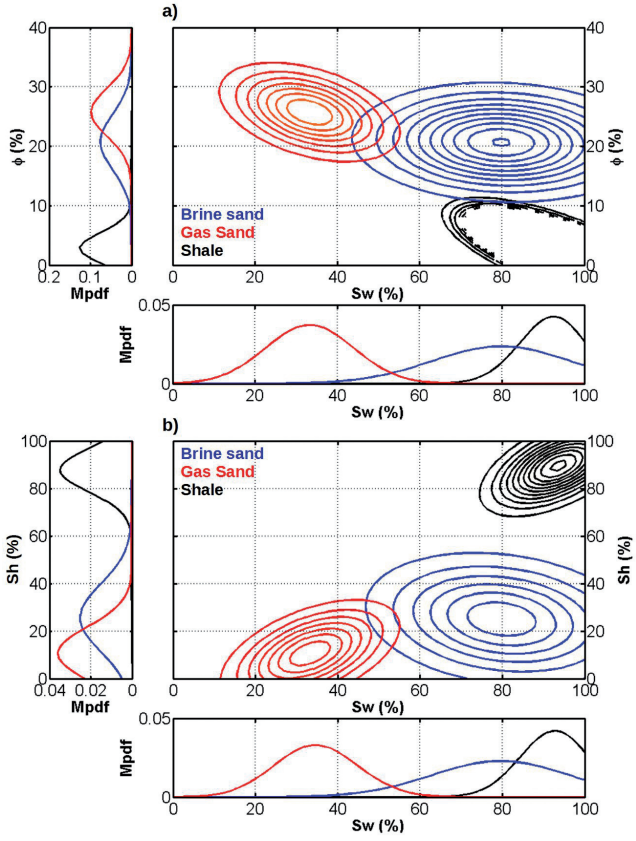

Fig. 1 – Prior probability distribution of the petrophysical variables (ϕ, *Sw* and *Sh*) computed taking into account three different litho-fluid classes: brine-sand, gas-sand and shale. The prior is distributed according to a Gaussian mixture model that allows us to take into account the multimodality and the correlation that usually characterize the distribution of the petrophysical properties in the subsurface (see Eq. 4). a) Prior distribution projected onto the Sw-ϕ plane and the associated marginal distributions (Mpdf) computed along the Sw and ϕ directions. b) Same as (a) but considering the *Sw-Sh* plane.

expectation maximization algorithm. Fig. 1 represents the prior Gaussian mixture distribution of water saturation, porosity and shaliness for the three facies. In Fig. 1a we represent the prior distribution projected onto the *Sw-ϕ* plane, together with the associated two marginal prior distributions (*Mpdf*) computed along the *Sw* and *ϕ* directions. As expected, the shale correspond to high *Sw* values and low porosity, whereas both brine sands and gas sands are characterized by higher porosity, with the gas sands at lower water saturation values than brine sands. Fig. 1b shows the prior distribution of the petrophysical properties projected onto the *Sw-Sh* plane. Similarly to Fig. 1a, the marginal distributions are also represented. As expected, the shales are characterized by higher shaliness values with respect to brine sands and gas sands.

To test the applicability of the petrophysical-seismic inversion and to check the reliability of the two considered rock-physics models, we show a synthetic inversion in which actual well-log measurements, pertaining to a well drilled in the target area, have been used to compute the synthetic seismic data. The synthetic data have been computed by means of a 1D convolutional forward modeling and using a 50 Hz Ricker wavelet as the source signature. Fig. 2a shows the synthetic CMP gather in which the offset has been converted to incident angles, whereas Figs. 2b, and 2c illustrate the results of the Bayesian AVA inversion. The green arrows in Fig. 2a at 2.46 s indicate the target gas-sand interval. The decrease of *Ip* and density and the increase of *Is* that characterize this gas-sand interval generate the typical class III AVA anomaly (Castagna and Swann, 1997) clearly visible in the synthetic seismogram. In Fig. 3a the blue curves depict the actual well-log data resampled at the seismic sample interval, the red curves illustrate the maximum a-posteriori (MAP) solution, and the gray curves are Monte Carlo realizations computed from the posterior distribution $p(m|d_{obs})$ (see Eq. 2). Each Monte Carlo realization represents a possible solution. As expected, the uncertainties increase passing from *Ip*, to *Is* and

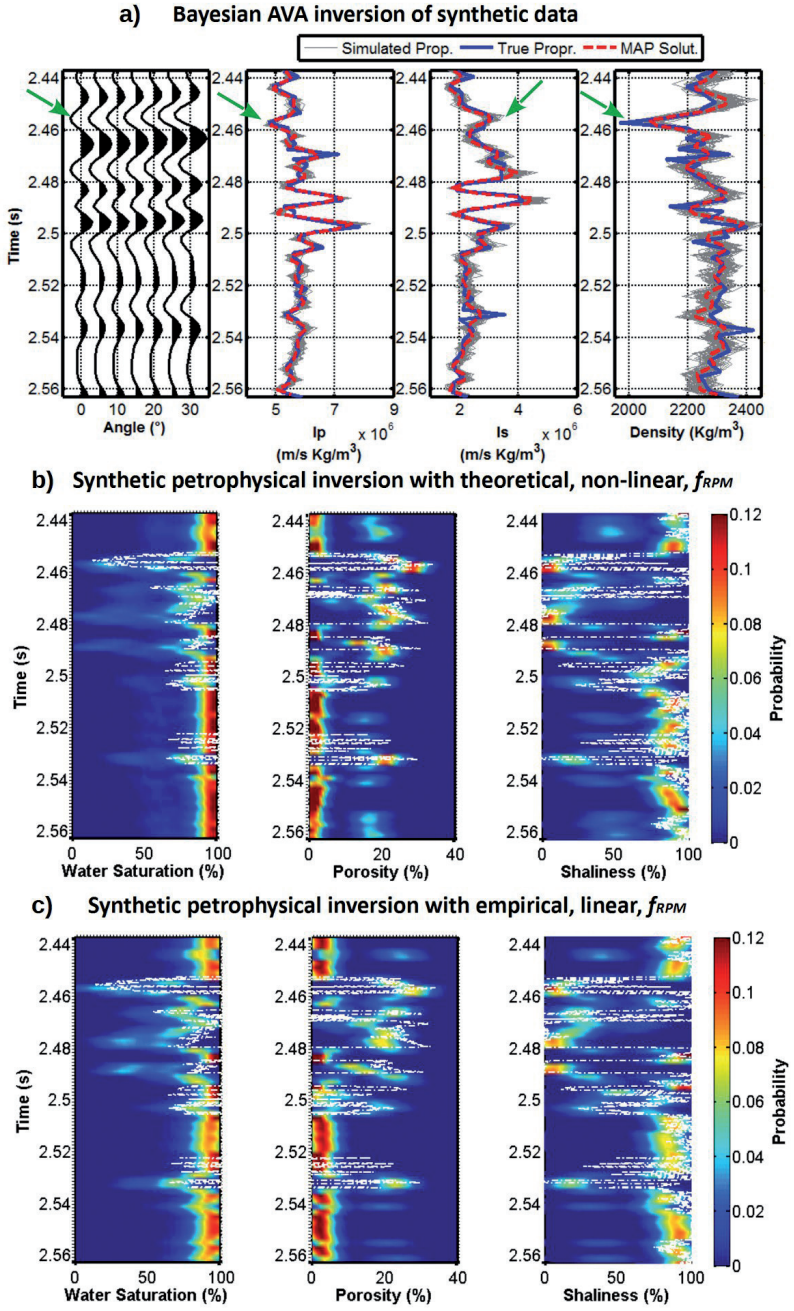

Fig. 2 – Results of the synthetic inversion based on actual well-log measurements. a) The synthetic CMP, P-impedance, S-impedance and density are represented from left to right. For impedances and density the x-axes are represented with the same scale to better illustrate the increase of uncertainty that occurs passing from the Ip, to the Is and to the density estimates. In blue are represented the true elastic properties, in red the maximum a posteriori (MAP) solution, whereas the grey curves show Monte Carlo samples form the posterior probability distribution. The green arrows indicate the target gas-sand that generates a class III AVA anomaly in the synthetic seismogram. b) and c) Results of the petrophysical inversion that is the posterior conditional probability $p(R|d_{obs})$ (see Eq. 11). The water saturation, porosity and shaliness are represented from left to right, respectively. b) Results obtained applying the theoretical, non-linear, rock-physics model. c) Results obtained with the empirical, linear, rock-physics model.

to density. However, we note that, although with a different resolution, the predicted elastic properties close match the true ones.

Now we move to describe the results of the petrophysical inversion obtained by applying both the linear, empirical, rock-physics model and the non-linear, theoretical, rock-physics model. The final, multimodal, Gaussian mixture distributions $p(R|d_{obs})$, derived for both the petrophysical inversions are represented in Figs. 2b and 2c. Fig. 2b shows the outcomes of the petrophysical inversion in which the theoretical, non-linear, rock-physics model (TPRM in the companion paper) has been considered, whereas Fig. 2c shows the results obtained when the empirical, linear, model (SR in the companion paper) has been used. In both cases we note that, as expected, the water saturation is poorly resolvable in the range 0-95% due to its minor influence in the *Ip* and *Is* values (although the main gas sand interval at 2.46 s has been correctly predicted), whereas the shaliness and, particularly, the porosity are well resolved. Comparing the predicted petrophysical properties with the true ones (shown by the dotted white lines), we note that, within the resolution of the seismic data, both the theoretical and the empirical rock-physics models are able to correctly predict the porosity and the shaliness values. In particular, both petrophysical inversions have been able to predict the many porosity and shaliness variations that occur between 2.45 and 2.50 s, where a finely layered sand-shale sequence occurs. As expected, a lower match between each predicted and true value and a higher uncertainty characterize the water saturation estimates. For the water saturation, we also note that the theoretical rock-physics model seems to produce a better fit with the true water saturation values with respect to the empirical rock-physics model. This fact can be ascribed to the difficulty of a linear rock-physics model to takes into account the non-linearity that characterizes the influence of the water saturation on the P and S impedances.

In conclusion, both the outcomes of the empirical, linear, and the theoretical, non-linear, rock-physics models show a fair match with the actual well-log measurements. This confirms the reliability and the applicability of the two rock-physics models in the petrophysical inversion. However, with respect to the analytical rock-physics model the theoretical model is more computer demanding as it requires a Monte Carlo simulation to compute the joint probability distribution $p(m,R)$. This peculiarity must be taken into account when the petrophysical inversion is performed on multiple CMP gathers.

The discussion about the field data inversion is limited to a single CMP location where a well-control is available. This CMP is the nearest to the well that has already been considered in the synthetic inversion. The seismic data have been processed paying particular attention at preserving the true amplitude of the reflections. However, due to the strong attenuation of high frequencies produced by several gas clouds occurring in the shallow layers, these seismic data are very poor in high frequencies. Consequently, the dominant frequency, at the depth of the target level, is around 15-18 Hz.

Fig. 3a illustrates the results of the Bayesian AVA inversion for the considered CMP gather. In the observed seismic data, despite the very low resolution, a clear class III AVA anomaly is visible at the target level (around 2.46 s). In blue are illustrated the true elastic properties resampled at the seismic sampling interval, the green lines show the true properties up-scaled to the seismic frequency band, the red curves represent the MAP solutions, while the gray lines are Monte Carlo realizations derived from the posterior distribution. As observed in the previous synthetic example the uncertainties increase passing from the impedances to the density estimates. However, the true up-scaled elastic properties (green lines) show a fair match with the estimated ones (red lines) and, more importantly, they lie inside the range defined by the Monte Carlo realizations.

Figs. 3b and 3c show the conditional probability distributions of the petrophysical properties predicted by using the theoretical, non-linear, and the empirical, linear, rock-physics models, respectively. At the low resolution of the seismic data, the differences in the results obtained with the two rock-physics models are negligible. Differently, from the previous synthetic test,

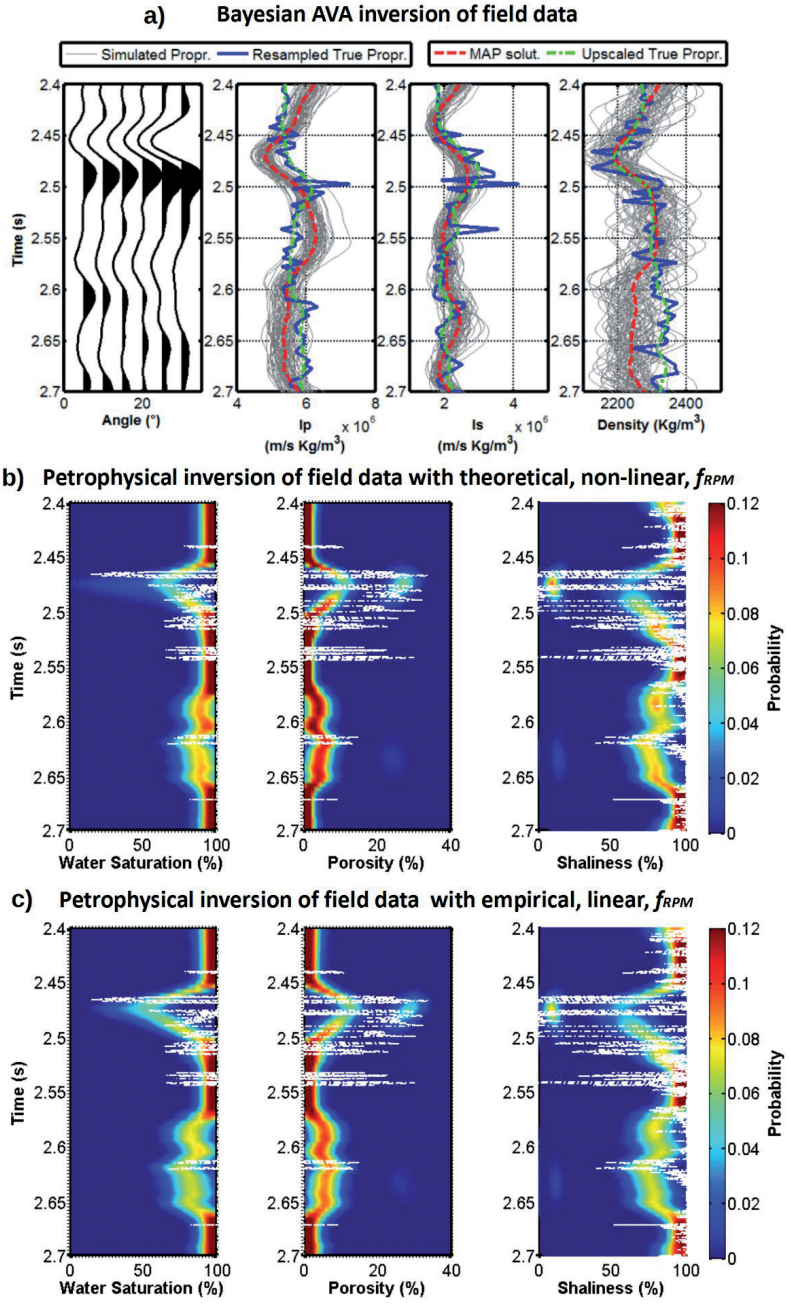

Fig. 3 – Results of the inversion of field data performed on the CMP location nearest to the well already considered in the synthetic inversion. a) The synthetic CMP, P-impedance, S-impedance and density are represented from left to right, respectively. For impedances and density the x-axes are represented with the same scale to better illustrate the increase of uncertainty that occurs passing from the Ip, to the Is and to the density estimates. In blue are represented the true elastic properties resampled at the seismic sampling interval, in red the MAP solution, in green the true properties up-scaled to the seismic bandwidth, whereas the grey curves show Monte Carlo realizations form the posterior probability distribution. b) and c) Results of the petrophysical inversion that is the posterior conditional probability $p(R|d_{obs})$ (see Eq. 11). The water saturation, porosity and shaliness are represented from left to right, respectively. b) Results obtained applying the theoretical, non-linear, rock-physics model. c) Results obtained with the empirical, linear, rock-physics model.

the low resolution of the seismic data makes a detailed characterization of the petrophysical properties in the subsurface impossible. However, despite the low-resolution issue, the petrophysical inversion has been able to predict the increase of porosity and the decrease of shaliness that occur between 2.45 and 2.50 s where the alternating shale-sand sequence occurs, but, differently from the synthetic inversion, this finely layered shale-sand sequence is resolved as a unique layer.

Conclusions. We presented a two-step probabilistic petrophysical inversion applied to reservoir characterization in offshore Nile delta. The first step of this procedure is a Bayesian linearized AVA inversion that returns the posterior probability distributions of the elastic properties (*Ip*, *Is* and density) in the subsurface. The second step is a probabilistic petrophysical inversion that makes use of the results of the previous AVA inversion, of the prior distribution of the petrophysical variables, and of a suitable rock-physics model to determine the posterior distribution of the petrophysical properties in the subsurface. This method propagates the uncertainties from seismic to petrophysical properties, including the effect of seismic noise error, the degree of approximation of the rock-physics model and the uncertainties that affect the estimated elastic properties. The Gaussian mixture model approach allows us to take into account the multimodality and the correlation that usually characterize the distribution of the petrophysical properties in the subsurface. The petrophysical inversion was performed making use of two different rock-physics models: a linear model (named SR in the companion paper) derived empirically by means of a stepwise regression from the available log data, and a non-linear model based on theoretical equations (named TRPM in the companion paper). Both rock-physics models returned very similar results, thus confirming their reliability and their applicability in the specific case under examination. The unique difference lies in the fact that the theoretical rock-physics model is more computer demanding as it requires a Monte Carlo simulation to compute the joint probability distribution $p(m,R)$. This peculiarity must be taken into account when applying the petrophysical inversion on multiple CMP locations.

The inversion of synthetic and field data confirmed the applicability of the proposed methodology. Shaliness and, particularly, porosity are the best resolved parameters. Conversely, water saturation in the range 0%-95% is poorly resolvable due to its minor influence on the *Ip* and *Is* values. The field data inversion was performed on a single CMP location where well-control was available to validate the results. The main limit of the seismic data is the very narrow frequency bandwidth that makes them unsuitable for detailed reservoir characterization studies.

The results of the Bayesian linearized AVA inversion have been also used to perform a probabilistic litho-fluid facies classification that makes use of Markov-chain models. For the lack of space, the outcomes of this classification procedure have not been discussed here.

Acknowledgments. The authors wish to thank EDISON for making the seismic and the well log data available and for the permission to publish this work.

References

Aki, K. and Richards, P.G.; 1980: *Quantitative Seismology: Theory and Methods*. WH Freeman & Co.

Avseth, P., Mukerji, T. and Mavko, G.; 2005: *Quantitative seismic interpretation: Applying rock physics tools to reduce interpretation risk*. Cambridge university press.

Buland, A. and Omre, H.; 2003: *Bayesian linearized AVO inversion*. Geophysics, 68(1), 185-198.

Castagna, J.P. and Swan, H.W.; 1997: *Principles of AVO crossplotting*. The leading edge, 16(4), 337-344.

Chiappa, F. and Mazzotti, A.; 2009: *Estimation of petrophysical parameters by linearized inversion of angle domain pre-stack data*. Geophysical Prospecting, 57(3), 413-426.

Grana, D. and Della Rossa, E.; 2010: *Probabilistic petrophysical-properties estimation integrating statistical rock physics with seismic inversion*. Geophysics, 75(3), O21-O37.

Hastie, T., Tibshirani, R., Friedman, J. and Franklin, J.; 2005: *The elements of statistical learning: data mining, inference and prediction*. The Mathematical Intelligencer, 27(2), 83-85.

Papoulis, A.; 1984: *Probability, random variables and stochastic processes*. McGraw-Hill.

Stolt, R. H. and Weglein, A. B.; 1985: *Migration and inversion of seismic data*. Geophysics, 50(12), 2458-2472.